CrystEngComm

PAPER

Cite this: *CrystEngComm*, 2017, **19**, 5882

Synthesis of a partially fluorinated ZIF-8 analog for ethane/ethene separation†

Suvendu Sekhar Mondal,[a] Maximilian Hovestadt,[b] Subarna Dey,[c] Carolin Paula,[b] Sebastian Glomb,[c] Alexandra Kelling,[a] Uwe Schilde,[a] Christoph Janiak,[c] Martin Hartmann[b] and Hans-Jürgen Holdt*[a]

Received 7th August 2017,
Accepted 20th September 2017

DOI: 10.1039/c7ce01438d

rsc.li/crystengcomm

The separation of ethane/ethene mixtures (as well as other paraffin/olefin mixtures) is one of the most important but challenging processes in the petrochemical industry. In this work, we report the synthesis of ZIF-318, isostructural to ZIF-8 but built from the mixed linkers of 2-methylimidazole (L1) and 2-trifluoromethylimidazole (L2) (ZIF-318 = $[(Zn(L1)(L2)]_n$). The synthesis has been optimized to proceed without ZnO-formation. Using only the L2 linker under solvothermal conditions afforded ZnO-embedded in the H-bonded and non-porous coordination polymer $ZnO@[Zn_2(L2)_2(HCOO)(OH)]_n$. The slight differences in the size of the substituents ($-CH_3$ *vs.* $-CF_3$) possibly in combination with different electronic inductive effects led to small but significant changes to the pore size and properties respectively, though the effective pore opening (aperture) size of ZIF-318 remained the same in comparison with ZIF-8. ZIF-318 is chemically (boiling water, methanol, benzene, and wide pH range at room temperature for 1 day), thermally (up to 310 °C) stable, and more hydrophobic than ZIF-8 which is proven by contact angle measurement. ZIF-318 can be activated for N_2, CO_2, CH_4, H_2, ethane, ethane, propane, and propene gases sorptions. Consequently, in breakthrough experiments, the ethane/ethene mixtures can be separated.

1. Introduction

Industrial C_2 to C_4 olefin/paraffin separations heavily rely upon energy intensive low temperature rectification technologies, which represent the most separation costly processes in the chemical industry. It is, therefore, highly desired to substitute the short chain paraffin/olefin separation by less energy-intensive separation techniques such as adsorption or membrane permeation. In principle, an adsorptive separation can be accomplished by kinetic or thermodynamic principles. Small differences in the molecular size can cause dramatic changes in the diffusion rates of the mixture components through molecular sieve pores, which lead in their extreme to the molecular sieve effect (size exclusion). Differences in the adsorptive interaction with the adsorbent allow equilibrium-based separations according to different mixed gas adsorption equilibria.

Zeolitic imidazolate frameworks (ZIFs)[1] are a subclass of MOF[2] materials which possess attractive structural properties and great potential for applications in gas storage,[3] chemical encapsulation and controlled delivery,[4] chemical sensing,[5] and gas separations,[6] including membrane-based separations.[7] ZIF-8, an iconic material which is the single most extensively studied ZIF material,[8] both from fundamental,[9] and from applied, functional perspective,[10] features sodalite (**sod**) topology with a high-void-volume and large spherical cavities but small apertures (*ca.* 3.4 Å diameter, if expansion *via* linker torsional motion is ignored), consisting of Zn(II) and 2-methyl-imidazolate (L1) ligand. A large number of studies for paraffin/olefin separations is devoted to ZIFs[11] and other metal carboxylates including CPO-27 (ref. 11*j* and 12) and MIL-53.[13]

For an efficient purification of the desired olefin, an adsorbent is required that has a higher affinity to the corresponding paraffin. In particular ZIF-8 has been extensively tested for paraffin/olefin separation employing ethane/ethene, propane/propene, *n*-butane/1-butene, and *n*-octane/1-octene mixtures. In all studies conducted so far, a higher paraffin selectivity has been observed.[11] Li *et al.* showed that the kinetic separation of propane/propene mixture can be tuned by the substituent (*e.g.*; CH_3, Cl and Br) of imidazole linker

[a] *Institut für Chemie, Anorganische Chemie, Universität Potsdam, Karl-Liebknecht-Straße 24-25, 14476 Potsdam, Germany. E-mail: holdt@uni-potsdam.de; Fax: +49 331 977 5055; Tel: +49 331 977 5180*
[b] *Erlangen Catalysis Resource Center (ECRC), Friedrich-Alexander-Universität Erlangen-Nürnberg, Egerlandstrasse 3, 91058 Erlangen, Germany*
[c] *Institut für Anorganische Chemie und Strukturchemie, Heinrich-Heine-Universität Düsseldorf, Universitätsstraße 1, 40225 Düsseldorf, Germany*

† Electronic supplementary information (ESI) available: Experimental details, IR-spectra, PXRD patterns, SEM images, TGA analysis, gas sorption data. CCDC 1495473 (CP-1) and 1495488 (ZIF-318). For ESI and crystallographic data in CIF or other electronic format see DOI: 10.1039/c7ce01438d

of ZIF-8 and its analog.[11g] In ZIF-8, the slightly smaller propene shows a diffusion coefficient which is about 125 times higher than that one of propane (at 303 K). The effective size of the pore opening and the framework flexibility were believed to be among the controlling factor determining the separation capability.[11g]

Hence, we are interested to modify the functionality of the imidazole linker of ZIF-8, with $-CF_3$, instead of $-CH_3$ which might enhance the flexibility of the ZIF-structure, character of pore apertures, and pore-size. Moreover, because of the highest electronegativity and extremely poor polarizability of fluorine atoms, fluorinated ZIF may exhibit unique physicochemical properties that can reflect gas sorption and separations. Recently, Zboril and Fischer *et al.* reported fluorinated graphene oxide and ZIF-8 composites for improved oil–water separation.[6c] A number of fluorine-containing linkers based hydrophobic MOFs are known,[14] and interestingly, solvent-assisted linker exchange in a series of ZIFs is reported by Farha, Hupp and co-workers.[10b] In this work, we report *de novo* synthesis of a new fluorinated ZIF $[Zn(L1)(L2)]_n$ (L2 = 2-trifluoromethyl-imidazolate) named as ZIF-318 which is isostructural with ZIF-8, exhibiting good gas sorption and ethane/ethene separations properties.

2. Experimental section

2.1. Materials and general methods

All solvents were used as purchased from commercial suppliers without further purification, if not stated otherwise. The linker precursors, 2-methylimidazole (L1) and 2-trifluoromethylimidazole (L2) were purchased from the chemical company TCI Europe and Activate Scientific, respectively. ZIF-8 was synthesized according to the published procedure.[1b] Optical images were taken by VWR Stereo Zoom Microscope. IR spectra were recorded on FT-IR Nexus from Thermo Nicolet in the region of 4000–400 cm^{-1} using KBr pellet. For X-ray structure determinations the crystals were embedded in perfluoropolyalkylether oil and mounted on a glass fibre. The data collections were performed on a STOE Imaging Plate Diffraction System IPDS-2 with graphite monochromatized Mo-Kα radiation at 50 kV and 40 mA ($\Delta\omega$ = 1°; CP-1: 210 K, 206 frames, 3 min exposure time per frame; ZIF-318: 180 K, 180 frames, 5 min exposure time per frame; see the ESI† for details). Powder X-ray diffraction patterns (PXRD) were measured on a Siemens diffractometer D5005 in Bragg–Brentano reflection geometry (see ESI† for details). Thermal gravimetric analysis (TGA) data were performed in a static air atmosphere from room temperature up to 900 °C with a Perkin Elmer TGA 4000 thermal analyzer. The heating rate was 10 °C min^{-1}. The samples were placed in ceramic pans. SEM-/EDX measurements were done on a JEOL JSM 6510 SEM equipped with an EDX spectrometer of Oxford (INCAx-act SN detector). For measurements of all samples were activated under vacuum by 200 °C for 24 hours and then coated with carbon (POLARON CC7650 Carbon Coater). Sessile drop contact angles of water on the samples were measured at room temperature about 10 s after placing the drop on the sample surface with a DSA 10 video contact angle measuring system G10 (Krüss, Germany), and data evaluation was done with software DSA version 1.80.02.

Solid-state NMR spectra were recorded on an Agilent 500 MHz wide bore spectrometer equipped with a 1.6 mm and a 3.2 mm probe. Larmor frequencies of ^1H and ^{13}C were 499.86 MHz and 125.71 MHz, respectively. ^1H single pulse magic-angle spinning (MAS) spectra were acquired in the 1.6 mm probe using a sample rotation frequency of 35 kHz and a 90 °C excitation pulse length of 1.4 μs. For each spectrum 64 scans were accumulated with a recycle delay of 5 s between the scans and an acquisition time of 15 ms. ^1H–^{13}C cross-polarization magic-angle spinning (CPMAS) experiments were done in a 3.2 mm rotor spinning the ZIF-318 sample at a rotation frequency of 18 kHz. In the ^1H–^{13}C CPMAS measurements a linear ramp was applied for the transfer of the polarization during a contact time of 4 ms. With a repetition delay of 5 s and high-power decoupling during acquisition 400 scans were collected for each spectrum. The measured ^1H and ^{13}C chemical shifts were referenced to adamantane. Liquid-phase ^{13}C NMR spectroscopy of activated ZIF-318 was recorded with a Bruker Advance 300 spectrometer. Resonances for NMR spectra are reported relative to Me_4Si (δ = 0.0 ppm).

2.2. Synthesis

Synthesis of ZnO@$[Zn_2(L2)_2(HCOO)(OH)]$ $(DMF)_{0.5}$ = CP-1. In a sealed tube (type A, company: Ace) 0.121 g (0.81 mmol) of 2-trifluoromethylimidazole (L2), and 0.342 g of $Zn(NO_3)_2 \cdot 4H_2O$ (0.81 mmol) were dissolved in 5 mL *N,N′*-dimethylformamide (DMF). The sealed tube was closed and the mixture was heated at 125 °C for 24 hours and was then allowed to cool down to room temperature with 5 °C per hour. A colorless crystalline material was formed. The fine crystalline product was washed with DMF and EtOH and dried in air. Yield for CP-1: 0.172 g (~55%) based on L2; IR (KBr pellet): ν_{max} = 3444 (m), 3342 (m), 3252 (m), 1650 (vs), 1587 (s), 1510 (s), 1285 (s), 1253 (m), 1100 (m), 1023 (m), 727 cm^{-1} (m).

Synthesis of [Zn(L1)(L2)] = ZIF-318. In a sealed tube (type A, company: Ace) 0.018 g (0.22 mmol) of 2-methylimidazole (L1), 0.031 g (0.22 mmol) of 2-trifluoromethylimidazole (L2), and 0.059 g of $Zn(NO_3)_2 \cdot 4H_2O$ (0.22 mmol) were dissolved in 3 mL of *N,N′*-diethylformamide (DEF). The sealed tube was closed and the mixture was heated at 135 °C for 48 hours and was then allowed to cool down to room temperature with 5 °C per hour. Light brown color crystals were washed with DEF and EtOH and dried in air. Under the same conditions with DMF solvent, light yellow crystals of ZIF-318 were also formed but with ZnO impurities. Single X-ray crystallographic measurement was done using the crystals, obtained under the same reaction conditions in DMF because of good diffraction quality (see ESI†). Yield for ZIF-318: 0.031 g (48.7% based on $Zn(NO_3)_2 \cdot 4H_2O$); IR (KBr pellet): ν_{max} = 3458 (m), 2931 (m), 1678 (s), 1581 (vs), 1461 (s), 1371 (s), 1309 (s), 1277 (s), 1226 (vs), 1185 (vs), 1144 (vs), 1098 (s), 1003 (vs), 954 (s), 828 (s), 745 cm^{-1} (vs).

2.3. Gas sorption measurements

N_2, CO_2, CH_4, H_2O and H_2 at 1 bar. Sorption isotherms were measured using a Micromeritics ASAP 2020 automatic gas sorption analyzer equipped with oil-free vacuum pumps (ultimate vacuum $<10^{-8}$ mbar) and valves, which guaranteed contamination free measurements. The sample was connected to the preparation port of the sorption analyzer and degassed under vacuum until the out gassing rate, *i.e.*, the rate of pressure rise in the temporarily closed manifold with the connected sample tube, was less than 2 μTorr min^{-1} at the specified temperature 200 °C for 24 h. After weighing, the sample tube was then transferred to the analysis port of the sorption analyzer. All used gases (H_2, He, N_2, CO_2, and CH_4) were of ultra high purity (UHP, grade 5.0, 99.999%) and the STP volumes are given according to the NIST standards (293.15 K, 101.325 kPa). Helium gas was used for the determination of the cold and warm free space of the sample tubes. H_2 and N_2 sorption isotherms were measured at 77 K (liquid nitrogen bath), whereas CO_2 and CH_4 sorption isotherms were measured at 298 ± 1 K (passive thermostating) 273.15 K (ice/deionized water bath) and 195.0 K (acetone/dry ice). The heat of adsorption value was done using the ASAP 2020 v3.05 software. Water sorption isotherms at 293 K were obtained volumetrically from a Quantachrome Autosorb iQ MP instrument equipped with an all-gas option.

Hydrocarbons. The adsorption isotherms of the gases ethane, ethene, propane and propene for ZIF-318 have been measured with a volumetric adsorption setup from micromeritics, called ASAP 2010. The temperature was adjusted by an external thermostat. The adsorbent has been activated at 220 °C under vacuum conditions for 24 hours prior to the adsorption experiment. The isotherm measurements have been carried out for the temperatures 10, 30 and 50 °C in a pressure region of 0 to 1 bar absolute. Between the measurements the sample was regenerated under vacuum conditions for several hours at a temperature of 110 °C.

Breakthrough experiments. For the dynamic separation experiments a single column adsorption setup was used at a constant temperature of 30 °C, with a constant feed flow of 1 ml_N min^{-1} and at atmospheric pressure. For the adsorption an equimolar composition of ethane and ethene and for desorption pure helium was used. The adsorber column was completely filled with ZIF-318. Additionally the ZIF-318 has been activated in a vacuum oven under 220 °C before mounting the column. After the assembly both adsorbents have been heated up to 100 °C while purging them with helium. The gas composition at the column outlet was analyzed by a gas chromatograph equipped with a flame ionization detector. The amount of the adsorbent was 0.6 g and the inner volume of the column was 0.9 cm^3.

3. Result and discussion

3.1. Synthesis, structure determination and characterization

To obtain L2 linker based ZIF structure, the reaction with L2 linker and $Zn(NO_3)_2{\cdot}4H_2O$ under solvothermal conditions in DMF failed to produce a ZIF-type structure. Instead ZnO embedded H-bonded coordination polymer (CP) ZnO@$[Zn_2(L2)_2(HCOO)(OH)]_n$, named as CP-1, was formed (Scheme 1). Interestingly, an equimolar amount of L2 and L1 with $Zn(NO_3)_2{\cdot}4H_2O$ under solvothermal reaction conditions at 135 °C in DMF yielded light brown crystals of ZIF-8 structure, designated as ZIF-318 along with ZnO impurities. The formation of ZnO is mainly due to the presence of an alkaline medium formed by the decomposition of DMF under relatively high temperature (see ESI† for details).[15] Surprisingly, if the same reaction was performed in DEF (Scheme 1 at ESI†), only phase pure ZIF-318 was formed and no ZnO impurity was detected.

The X-ray structural analysis shows that CP-1 crystallizes in the orthorhombic crystal system with the space group *Pnma*.[16] The asymmetric unit consists of one Zn(II) ion, one L2 ligand, hydroxido ion (OH^-), half of a formate ion ($HCOO^-$), and a non-coordinated DMF molecule as illustrated in Fig. S3 (in the ESI†). The crystal structure of CP-1 has the neutral 2D network $[Zn_2(L2)_2(HCOO)(OH)]_n$ where Zn atoms are bridged by the L2 linker, and OH^- and $HCOO^-$, respectively. The hydroxido and carboxylato bridging action results in a six membered di-metallacycle (Fig. 1a). The Zn(II) ion is tetrahedrally-coordinated by two donor N atoms (N1 and N2) of two L2 ligands, one bridging OH^- (O1) and one oxygen atom (O2) from $HCOO^-$. Each of this six-membered $\{Zn_2(\mu\text{-}HCOO)(\mu\text{-}OH)\}$ rings is connected by coordinating with the N (N1 and N2) atoms of L2 ligands with Zn, forming 2D hexagonal ring-containing corrugated honeycomb layers of **hcb** (6^3) topology parallel to the *ab* plane (Fig. 1b). Adjacent layers are shifted relative to each other and stacked along the *a* axis by classical O–H···O and non-classical weak C–H···O/F hydrogen-bonding interactions, forming a supramolecular 3D framework (Fig. 1c and Table S2 in the ESI†) with channels filled with DMF molecules as solvent (Fig. 1d). The as-synthesized CP-1 contains 4 DMF molecules per unit cell and half a DMF per asymmetric unit (ESI† for details).

Single crystal X-ray diffraction revealed that ZIF-318 is isostructural with ZIF-8, both crystallizing in the cubic space group $I\bar{4}3m$ with almost identical unit cell constants (see ESI† for details).[17,1b] Zinc centers are tetrahedrally coordinated to four N atoms from two L1 and two L2 ligands as Zn(L1)(L2) in the **sod** topology. The square faces of the sodalite cages are essentially blocked by the fluorine atoms (Fig. S5†); therefore, the cages are interconnected along 3-fold axes through the small hexagonal openings, considering the vander-Waals surfaces of the H atoms on the imidazolate (Im) ligands (Fig. 2a). However, the slight differences in the sizes of the substituents and possibly in combination with different electronic inductive effects lead to small but significant perturbations to the Zn–N bond distances (d), Zn–Im–Zn angles (θ), the dihedral angles between the imidazole ring and the hexagonal faces enclosed by 6 zinc centers (Φ), as well as Zn–Zn distances (L), which result in only slightly different effective pore opening (window, aperture) sizes (A), (Fig. 2b and Table 1) and pore size (D) of ZIF-318 relative to ZIF-8. The pores of the as-synthesized ZIF-318 contain 2 DMF molecules

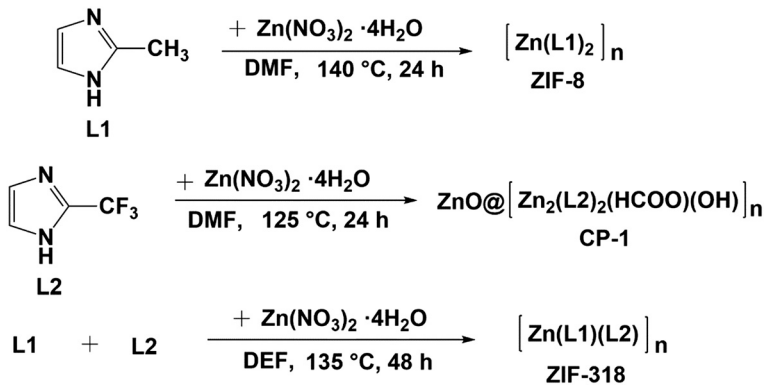

Scheme 1 Solvothermal synthesis of partially fluorinated ZIF-8 analog ZIF-318.

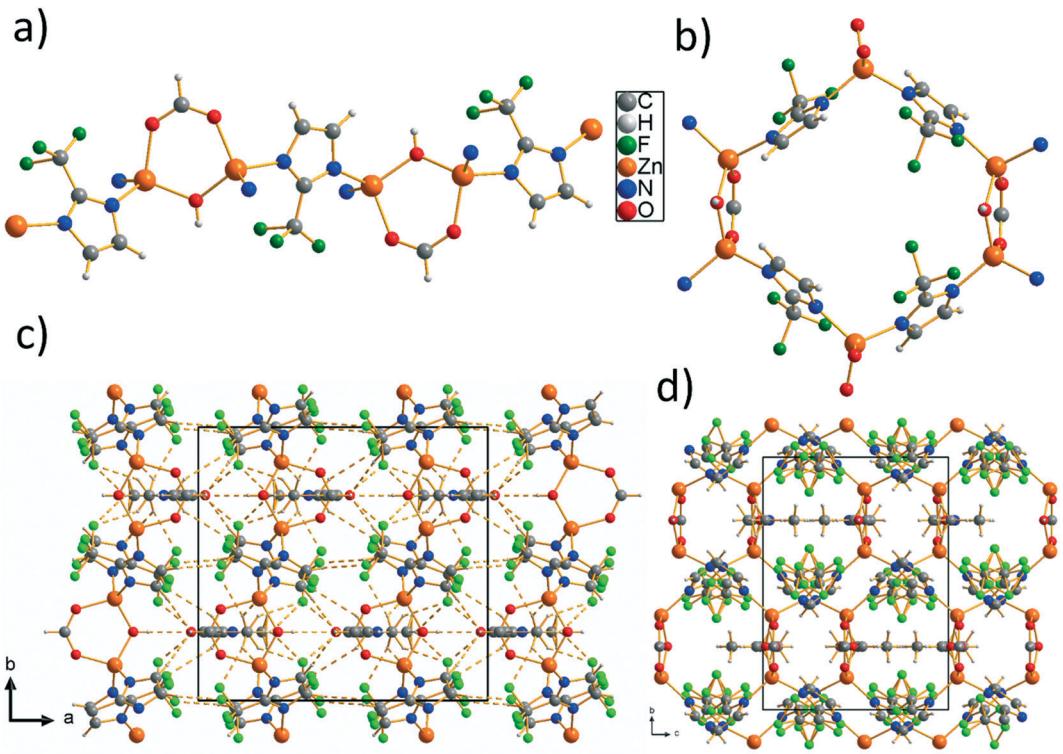

Fig. 1 CP-1; a) 1D chain, with 6-membered di-metallacycle; b) 2D hexagonal ring; c) H-bonds between layers; d) DMF solvent occupied, H-bonded CP-1.

per formula unit, in a solvent-accessible void volume of 46% of the unit cell volume (see ESI† for details). As expected the result of higher van der Waals radii of fluorine (1.47 Å) than hydrogen (1.20 Å), lower pore size (D) have been observed in ZIF-318 (10.6 Å) than in ZIF-8 (11.6 Å), despite their similar structure. Scanning electron microscopy (SEM) image revealed small particles with similar morphologies of ZIF-8 (Fig. 2c). Elemental mapping of the crystal showed a homogeneous zinc and especially fluorine distribution (Fig. 2d and e). The as-synthesized material was confirmed by PXRD patterns (Fig. 2f). To examine the architectural, thermal, and chemical stability and porosity of ZnO free ZIF-318, we prepared at the gram scale, using in DEF solvent to allow detailed investigation of the aforementioned properties.

The chemical stability of ZIF-318 was analyzed by suspending the sample for 24 hours in boiling methanol, benzene and water, conditions that reflect extreme operational parameters of typical industrial chemical processes. After such extensive treatment, ZIF-318 maintained crystalline integrity as confirmed by PXRD patterns (Fig. S7†). Additionally, the chemical stability of ZIF-318 was then tested by treating its samples under different pH conditions (pH = 1.5 to 12.0) at room temperature for 1 day. It was found that the PXRD patterns of all treated ZIF-318 remain intact, which indicated there was no phase transition or framework collapse during treatments (Fig. S8†). TGA trace for ZIF-318 in air atmosphere indicated a gradual weight-loss step of 7.6% (25–300 °C), corresponding to partial loss of DEF, followed by

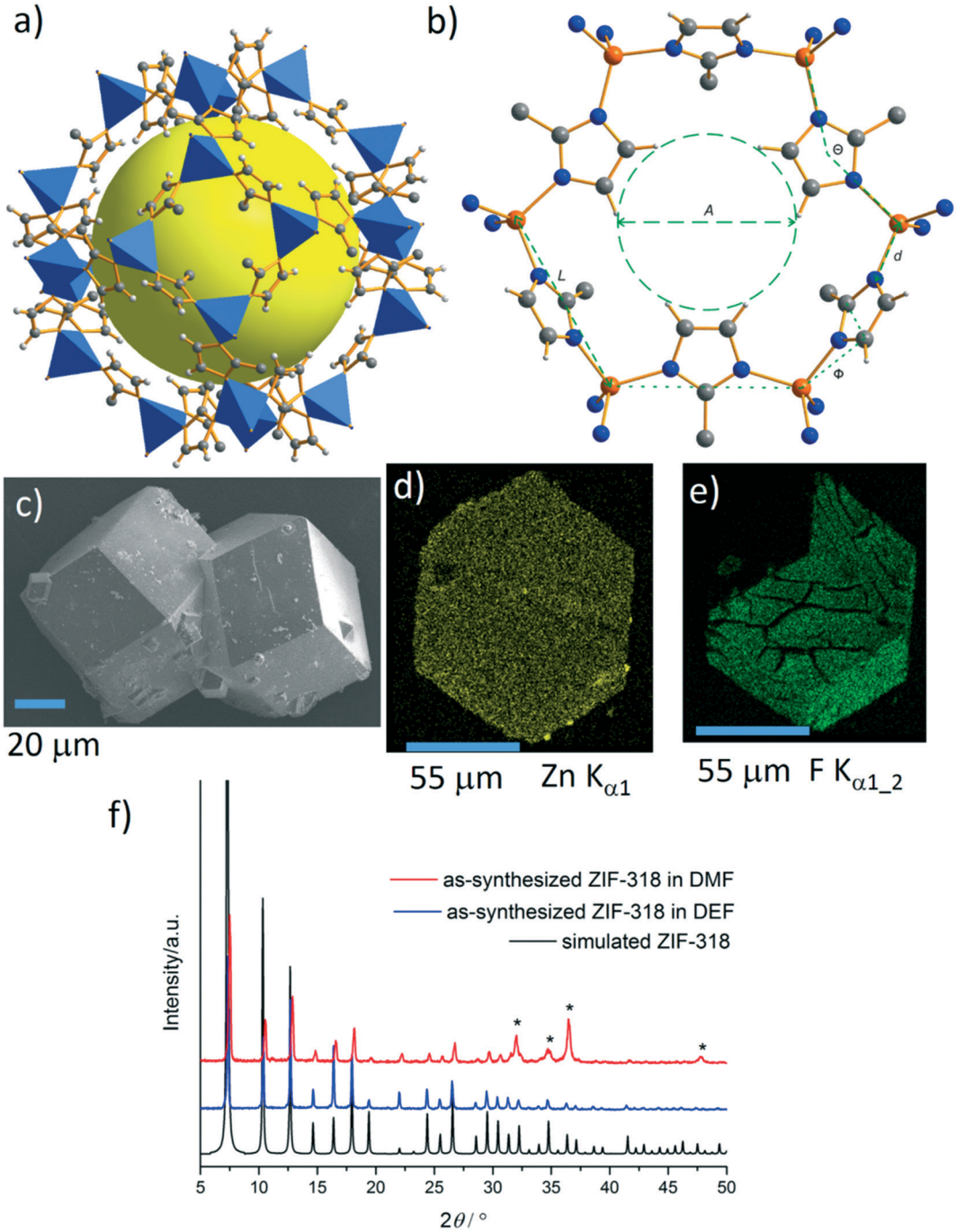

Fig. 2 a) View of the pore of ZIF-318 (yellow sphere indicates the cavity inside the cages (~10.6 Å in diameter, taking into account the van der Waals radii of the surrounding atoms); b) labelling scheme of the structural features determining the pore opening size; C2 position of imidazole linker is half occupied by the substituent of $-CH_3$ and $-CF_3$, respectively, as proven by single crystal X-ray diffraction (see ESI† for details); C: gray; H: light gray; N: blue; Zn: orange; F: green; c) scanning electron micrograph (SEM) for ZIF-318; element mapping ZIF-318 d) for zinc; e) for fluorine (it was observed that passing of high electron beam created the creaking of the crystal. Also, F mapping of one face of the crystal was missing. We suspect that the electron beam comes from the opposite side of the crystal face; therefore electrons can not recognize the out-going face); and f) PXRD patterns of ZIF-318, synthesized in DMF and DEF. Difference in the relative intensities is because of the simulated pattern does not account for the disordered solvent molecules in the pores. The star marks (*) are assigned to diffraction peaks of ZnO phase.

decomposition of the framework (Fig. S9†). The TGA trace of activated ZIF-318 showed a long plateau up to 310 °C, indicating higher thermal stability in the absence of guest molecules. To examine its hydrophobic properties, we carried out contact-angle measurements on the states of the degassed sample of pressed pellet, in comparison with ZIF-8. A pellet of pristine ZIF-8 showed a water contact angle of about 45° (Fig. S12†). ZIF-318 exhibited a water contact angle of 68.4°

Table 1 Structural factors determining the effective diameter of the pore windows, *(A)* and pore diameter *(D)* of ZIF-318

ZIF	θ (deg)	d (Å)	Φ (deg)	L (Å)	A (Å)	D (Å)
ZIF-318	147	1.99	12.1	6.04	3.4	10.6
ZIF-8 (ref. 1*b* and 11*g*)	145	1.98	10.8	6.02	3.4	11.6

θ = Zn–Im–Zn angles. d = Zn–N bond distances. Φ = the dihedral angles between the imidazole ring and the hexagonal faces enclosed by 6 zinc. L = centers. Zn–Zn distances. A = effective pore opening (aperture) diameter. D = pore diameter.

(hydrophobic nature) due to the high proportion of covalent C–F bonds of the fluorinated aromatic ligand.

Solvent exchanged of ZIF-318 was carried out by Soxhlet extraction with dry methanol over 3 days. The solvent-exchanged material was activated by degassing at 220 °C under high vacuum (10^{-6} Torr) for 24 hours, prior to gas-sorption measurements. This activation procedure and the purity can be confirmed by the solid-state ^{1}H–^{13}C CP MAS NMR spectroscopy (Fig. S13†). Besides the characteristic signals of L1 in ZIF-8 at 13.9, 124.4 and 151.1 ppm, also peaks of L2 at 118.2, 120.2, 127.1 and 142.8 ppm appear. In contrast to the liquid-phase ^{13}C NMR measurements (Fig. S14†) and the solid-state ^{1}H–^{13}C CPMAS experiments, in the ^{1}H MAS NMR spectra small and sharp solvent peaks of DEF are additionally visible at 0.4 (–CH_3), 2.6 (–CH_2–) and 7.3 ppm (–N–CO–H). The signals at 1.8 (–CH_3) and 6.8 ppm (–CH═) feature resonance frequencies of standard ZIF-8. The presence of the DEF peaks solely in the ^{1}H MAS NMR spectra reveals that there is only a very little amount of remaining solvent in the pores of activated ZIF-318. Moreover, the activated sample maintained its crystalline integrity, as indicated in the PXRD pattern (Fig. S7†).

3.2. Gas sorption and separation properties

The N_2 adsorption/desorption isotherms at 77 K up to a relative pressure p/p_0 of 0.995, exhibit a reversible type-I(a) characteristics with a very small *H4*-type hysteresis loop in the 0.45–1.0 p/p_0 range (Fig. 3) which may be attributed to mesopores from the aggregated ZIF crystallites.[18] There is only a very small residual uptake over a range of high p/p_0. For N_2 at 77 K, type I(a) isotherms are observed for microporous materials having mainly narrow micropores (of width $< \sim 1$ nm). The estimated Brunauer–Emmett–Teller (BET) surface area and the Langmuir surface area are 835 $m^2\ g^{-1}$ and 1007 $m^2\ g^{-1}$, respectively. Such surface area is comparable and higher than those for ZIF-69, −78, −79, −81, and −100;[1] but lower than ZIF-8 (1900 $m^2\ g^{-1}$, Fig. S16†) at the same experimental conditions, though, the value is highly dependent on the preparation and activation methods employed.[8,1b] The total pore volume is 0.37 $cm^3\ g^{-1}$ (from "N_2 DFT slit pore" model of N_2 sorption data at 77 K). For the sample of ZIF-8 the total pore volume was 0.80 $cm^3\ g^{-1}$ for pores smaller than 41 nm diameter at p/p_0 = 0.95. The narrow pore-size distribution is centered around a maximum at 9.3 Å (NL-DFT methods; Fig. 3, inset) that can be comparable with pore size obtaining from the crystal structure data (10.6 Å).

The CO_2 adsorption capacities in activated ZIF-318 are 36.4 $cm^3\ g^{-1}$ at 273 K and 16.5 $cm^3\ g^{-1}$ at 298 K and 1 bar (Fig. 4a) broad desorption hysteresis were observed. The CO_2 uptake in activated ZIF-8 is 47.4 $cm^3\ g^{-1}$ at 273 K and 1 bar (Fig. 4b) with the similar desorption hysteresis. The slightly more dominant hysteresis for ZIF-318, esp. at 298 K could be evidence for the increased flexibility of the linkers resulting in pore blocking effects. The methane sorption capacities of ZIF-318 and ZIF-8 were estimated to be 7.3 and 18.6 $cm^3\ g^{-1}$, respectively at 273 K (Fig. S17†). ZIF-318 adsorbs 122 $cm^3\ g^{-1}$ of H_2 at 77 K and 1 bar; but lower than ZIF-8 (163.8 $cm^3\ g^{-1}$, Fig. S18†).[1b] The difference in CO_2, CH_4 and H_2 uptake between ZIF-318 and ZIF-8 follows the difference in surface area and pore volume which is both almost twice for the sample of ZIF-8 over ZIF-318. To further understand the adsorption properties, the isosteric heats of adsorption were calculated from the CO_2 adsorption isotherms at 273 and 298 K (Fig. S19†). At zero loading the Q_{st} value (−ΔH) is 23 kJ mol^{-1}. Upon increasing the loading the Q_{st} value decreases rapidly to 14 kJ mol^{-1}. Notably, the adsorption enthalpy decreased at first, and finally increases with increasing CO_2 uptake that might suggest strong interaction with –CF_3 groups of the linkers of ZIF-318. ZIF-318 shows a water vapour uptake of 29 cm^3 (STP) g^{-1} or 0.023 g g^{-1}, which is slightly higher than for ZIF-8 (17 cm^3 (STP) g^{-1} or 0.014 g g^{-1}), at a relative pressure (p/p_0) of 0.9 at 293 K (Fig. 4c and d), and lower than MIL-100(Al) (0.5 g g^{-1}), MIL-100(Fe) (0.65–0.75 g g^{-1}),[19] Al-fumarate (0.45 g g^{-1}),[20] CAU-10-H (0.33–0.34 g g^{-1}),[21] MIL-

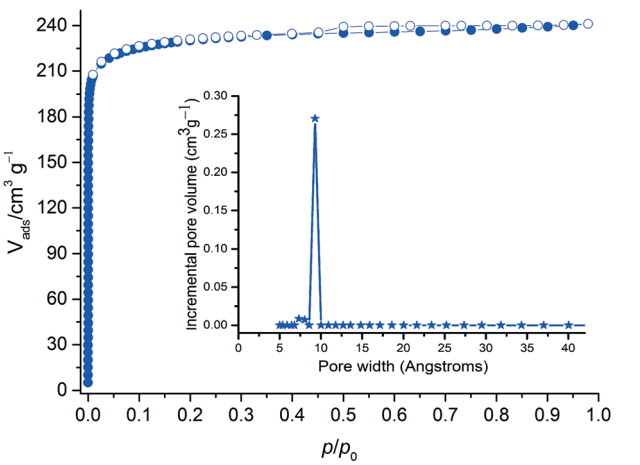

Fig. 3 N_2 sorption isotherm at 77 K (at inset, pore size distribution) of ZIF-318 (adsorption and desorption branches are indicated in closed and open symbols, respectively).

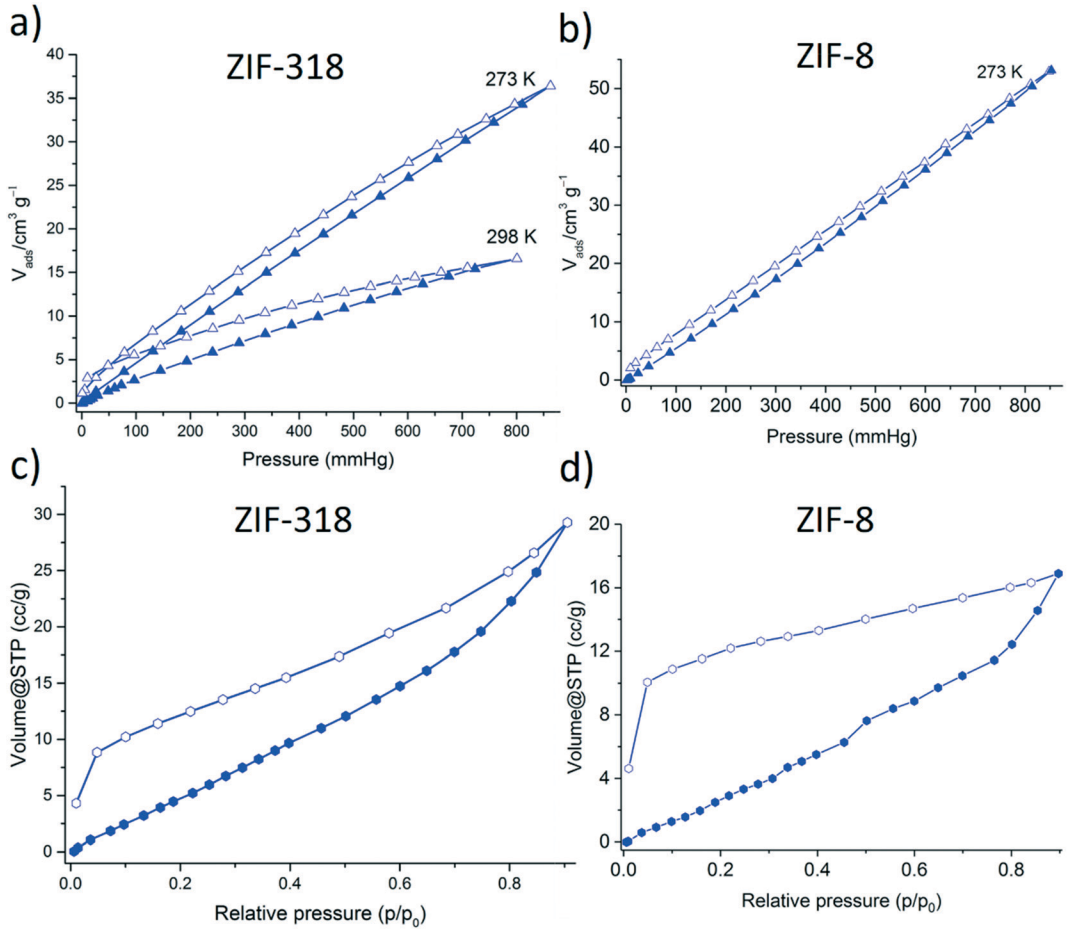

Fig. 4 a) CO_2 sorption isotherms for ZIF-318; b) CO_2 of ZIF-8; c) water sorption isotherm of ZIF-318; d) water sorption isotherm for ZIF-8 at 293 K (adsorption and desorption branches are indicated with closed and open symbols, respectively).

101(Cr) (1.0–1.5 g g^{-1}).[22] The water uptake of both ZIF-318 and ZIF-8 is low as can be expected from their hydrophobic nature. Still, the order in water uptake capacity with ZIF-8 < ZIF-318 is counterintuitive in view of the order in porosity, the above gas uptake capacities and contact angle measurements. To understand this incongruity, a number of hydrophobic MOFs based on (long-chain) alkyl substituents and/or fluorine-containing MOF (F-MOF) is taken into account.[14] For example, Omary *et al.* presented a series of F-MOFs with notable hydrophobicity for the adsorption of aromatic and aliphatic components of oil.[14d] Comparing the results of water contact angle measurements of the ZIFs and the fluorinated ZIF (synthesized by solvent assisted linker exchange (SALE)) materials by Hupp, Farha and co-workers revealed that significantly larger contact angles for the fluorinated ZIF.[10b] In contrast to the contact-angle measurements, vapor sorption measurements showed no enhancement of the hydrophobicity for fluorinated ZIF relative to ZIF-69. Also, Kitagawa and coworkers mentioned that without the use of alkylation or fluorination of MOF adsorbed water vapor despite its superhydrophobicity.[14a] Contact-angle measurements are exclusively on interactions of the exterior surfaces of materials wherein the water vapor sorption is totally an interior pore surfaces properties and in fact, depends on how much the pore is hydrophilic. The contrast between these two results can likely be attributed to the cohesive forces between water molecules, resulting in higher surface tension in the contact-angle measurements. This hypothesis is proven by a hydrophobic F-MOF where the incorporation of water and formation of water clusters in the hydrophobic cavities of a fluorinated MOF were studied.[23] It has been mentioned that the interaction with the fluorine-decorated channels is the weakest; instead, hydrogen bonding of the water species dominates, leading to clustering. The hydrophobic environment of the MOF creates the ideal conditions for the stabilization of these water clusters as compared to the unconstrained case.[23] These reported studies can explain the water vapor sorption behavior in spite of showing higher water contact-angle of ZIF-318. The desorption isotherms of ZIF-8 and -318 showed a broad hysteretic behavior, which could signal water coordination to available Zn coordination sites from linker defects. Thus, the slightly higher water uptake in ZIF-318 could also be due to an increased number of linker defects and concomitant coordinately unsaturated Zn sites. CP-1 was proven non-porous due to instability of H-bonds.

The shapes of the adsorption isotherms of the light hydrocarbons on ZIF-318 at 303 K (Fig. 5a) are quite similar to the results of ZIF-8 reported in the literature.[11h] However, the capacity of ZIF-318 is lower compared to that of ZIF-8,[11h] which amounts to 2.5 mmol g^{-1} and 1.5 mmol g^{-1} for ethane and ethene, respectively. This is in line with the lower surface area of 835 m^2 g^{-1} determined for ZIF-318 as compared to ZIF-8 (1900 m^2 g^{-1}). When the ethane or ethene loading is calculated per mol zinc, no difference in the respective adsorption isotherm is observed. For ethane and ethene, an almost linear increase in the uptake and no saturation plateau is observed up to a pressure of 1 bar. Moreover the uptake of the ethane is higher (1.25 mmol g^{-1}) compared to the ethene (1 mmol g^{-1}). For propane and propene higher uptakes (up to 2.75 mmol g^{-1}) are observed but the isotherms are too close to detect a certain preferred adsorption. From the ratios of the initial slopes in the Henry region of the adsorption isotherms, the olefin/paraffin selectivities are calculated. Compared to the results of ZIF-8, the selectivity of ZIF-318 at zero loading is lower with $\alpha_{ethane/ethene}$ = 1.43, but in the range of ZIF-8 with $\alpha_{ethane/ethene}$ = 1.78.[11h] In the work of Zhang *et al.*, the isotherms of ZIF-8 show a higher selectivity at 308 K ($\alpha_{propane/propene}$ = 1.34) compared to ZIF-318 at 303 K ($\alpha_{propane/propene}$ = 1.14).[11b]

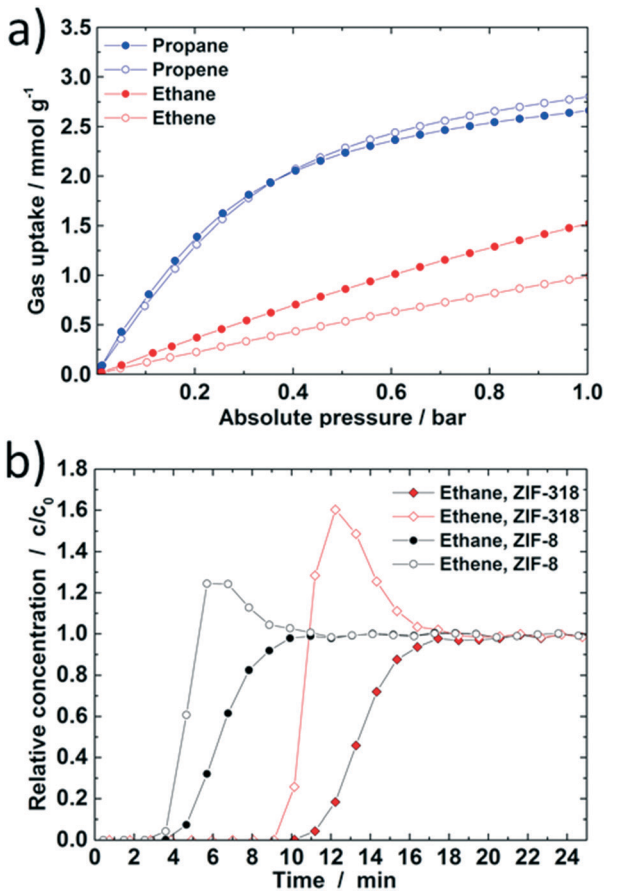

Fig. 5 a) Single compound adsorption isotherms of ethane, ethene, propane and propene at 303 K; b) adsorption of a binary breakthrough experiment with an equimolar mixture of ethane and ethene at 303 K using ZIF-318 and ZIF-8 as adsorbent.

The breakthrough experiment of an equimolar mixture of ethane and ethene using ZIF-318 and ZIF-8 at 303 K (Fig. 5b) shows the typical shape for the separation of a binary mixture. First ethene leaves the column, followed by the stronger adsorbing component ethane, this fits to the pure isotherm measurements at 303 K plotted in Fig. 5a and as reported in the literature for ZIF-8 literature.[11h] The difference in retention time is to some extent related to the different amount of adsorbent in the same adsorber volume, *viz.* 0.5955 g of ZIF-318 and 0.153 g of ZIF-8. However, the separation with ZIF-318 is more efficient compared to ZIF-8 because of the larger time interval where pure ethene is recovered from the column. Therefore ZIF-318 is well suited for the separation of ethane/ethene mixtures in continuous gas separation processes.

4. Conclusion

In summary, a 2-methylimidazolate and 2-trifluoromethylimidazolate mixed-linker based ZIF-8 type framework, named here ZIF-318 was synthesized, characterized and examined for its potential in the paraffin/olefin separation. ZIF-318 is proven chemically stable in boiling water, methanol and benzene as well as stable over a wide pH (pH = 1.5–12.0) range at room temperature for 1 day. ZIF-318 shows half of the BET surface area and lower pore volume than ZIF-8 due to bigger size of the fluorine over hydrogen atoms of the CF_3 group, though the hexagonal pore apertures, determined by the imidazole C4-H and C5-H atoms remain nearly the same for both ZIFs. CO_2 and H_2 uptake capacities are comparable with other ZIFs; but lower than ZIF-8 because of the aforementioned lower BET surface area and pore volume. Single-component adsorption isotherms of ethane, ethene, propane, and propene were measured. The olefin/paraffin selectivities are calculated from the single hydrocarbon isotherms at zero loading. In addition, the separation behavior was investigated in breakthrough-curve experiments for ethane/ethene mixtures, showing that ZIF-318 could be suitable for ethane/ethene mixture gas separation in continuous gas separation processes. We realize that the rich organic chemistry could still provide us with other useful organic linker to construct new porous zeolitic imidazolate framework, like ZIF-318 of their diverse applications in the near future. Also, we note that the synthesis of mixed-ligand approach by varying mole ratios could further light on the comparison between the two MOFs. Such comparison is, however, beyond the scope of the present proof-of-principle study and will be addressed in follow-up work. Mixed-organic ligands, that is, mixed linkers in MOFs are of current interest.[24] It is evident to fine-tune the properties by using mixtures of two types of organic linker molecules. This mix-MOF concept, where one of the two linkers is only used for building the framework structure while the other is providing additional functional side group(s) and controlling pore properties, has been

demonstrated for MOF-5,[25] MIL-101(Cr),[26] H_2N-MIL-101(Al),[27] MIL-53(Al)[28] and ZIFs.[29]

Conflicts of interest

There are no conflicts to declare.

Acknowledgements

The authors thank Dr. Klaus Tauer (Max Planck Institute of Colloids and Interfaces, Potsdam, Germany) for the contact-angle measurement. This work is financially supported by the German Research Foundation (SPP 1362 "Porous Metal–Organic Frameworks," HO 1706/7-1, HO 1706/7-2 and SPP1570, HA2527/-12-3).

References

1 (*a*) A. Phan, C. J. Doonan, F. J. Uribe-Romo, C. B. Knobler, M. O'Keeffe and O. M. Yaghi, *Acc. Chem. Res.*, 2010, **43**, 58–67; (*b*) K. S. Park, Z. Ni, A. P. Côté, J. Y. Choi, R. Huang, F. J. Uribe-Romo, H. K. Chae, M. O'Keeffe and O. M. Yaghi, *Proc. Natl. Acad. Sci. U. S. A.*, 2006, **103**, 10186–10191; (*c*) R. Banerjee, H. Furukawa, D. Britt, C. Knobler, M. O'Keeffe and O. M. Yaghi, *J. Am. Chem. Soc.*, 2009, **131**, 3875–3877; (*d*) N. T. T. Nguyen, H. Furukawa, F. Gándara, H. T. Nguyen, K. E. Cordova and O. M. Yaghi, *Angew. Chem., Int. Ed.*, 2014, **53**, 10645–10648.

2 (*a*) H.-C. Zhou, J. R. Long and O. M. Yaghi, *Chem. Rev.*, 2012, **112**, 673–674; (*b*) H.-C. Zhou and S. Kitagawa, *Chem. Soc. Rev.*, 2014, **43**, 5415–5418; (*c*) E. López-Maya, C. Montoro, L. M. Rodríguez-Albelo, S. D. A. Cervantes, A. A. Lozano-Pérez, J. L. Cenís, E. Barea and J. A. R. Navarro, *Angew. Chem., Int. Ed.*, 2015, **54**, 6790–6794; (*d*) Z. Wei, Z.-Y. Gu, R. K. Arvapally, Y.-P. Chen, R. N. McDougald Jr, J. F. Ivy, A. A. Yakovenko, D. Feng, M. A. Omary and H.-C. Zhou, *J. Am. Chem. Soc.*, 2014, **136**, 8269–8276; (*e*) K. Leus, P. Concepcion, M. Vandichel, M. Meledina, A. Grirrane, D. Esquivel, S. Turner, D. Poelman, M. Waroquier, V. Van Speybroeck, G. Van Tendeloo, H. García and P. Van Der Voort, *RSC Adv.*, 2015, **5**, 22334–22342; (*f*) A. Bhunia, S. Dey, J. M. Moreno, U. Diaz, P. Concepcion, K. Van Hecke, C. Janiak and P. Van Der Voort, *Chem. Commun.*, 2016, **52**, 1401–1404.

3 R. Banerjee, A. Phan, B. Wang, C. Knobler, H. Furukawa, M. O'Keeffe and O. M. Yaghi, *Science*, 2008, **319**, 939–943.

4 (*a*) S. Li, K. Wang, Y. Shi, Y. Cui, B. Chen, B. He, W. Dai, H. Zhang, X. Wang, C. Zhong, H. Wu, Q. Yang and Q. Zhang, *Adv. Funct. Mater.*, 2016, **26**, 2715–2727; (*b*) H. Zheng, Y. Zhang, L. Liu, W. Wan, P. Guo, A. M. Nyström and X. Zou, *J. Am. Chem. Soc.*, 2016, **138**, 962–968; (*c*) W. Li, Y. Zhang, Z. Xu, Q. Meng, Z. Fan, S. Ye and G. Zhang, *Angew. Chem., Int. Ed.*, 2016, **55**, 955–959.

5 (*a*) J.-W. Ye, H.-L. Zhou, S.-Y. Liu, X.-N. Cheng, R.-B. Lin, X.-L. Qi, J.-P. Zhang and X.-M. Chen, *Chem. Mater.*, 2015, **27**, 8255–8260; (*b*) C. G. Jones, V. Stavila, M. A. Conroy, P. Feng, B. V. Slaughter, C. E. Ashley and M. D. Allendorf, *ACS Appl. Mater. Interfaces*, 2016, **8**, 7623–7630; (*c*) C. Mottillo and T. Friščić, *Angew. Chem., Int. Ed.*, 2014, **53**, 7471–7474.

6 (*a*) H. T. Kwon, H.-K. Jeong, A. S. Lee, H. S. An and J. S. Lee, *J. Am. Chem. Soc.*, 2015, **137**, 12304–12311; (*b*) K. Eum, K. C. Jayachandrababu, F. Rashidi, K. Zhang, J. Leisen, S. Graham, R. P. Lively, R. R. Chance, D. S. Sholl, C. W. Jones and S. Nair, *J. Am. Chem. Soc.*, 2015, **137**, 4191–4197; (*c*) K. Jayaramulu, K. K. R. Datta, C. Rösler, M. Petr, M. Otyepka, R. Zboril and R. A. Fischer, *Angew. Chem., Int. Ed.*, 2016, **55**, 1178–1182.

7 (*a*) H. Bux, F. Liang, Y. Li, J. Cravillon, M. Wiebcke and J. Caro, *J. Am. Chem. Soc.*, 2009, **131**, 16000–16001; (*b*) H. B. Tanh Jeazet, S. Sorribas, J. M. Román-Marin, B. Zornoza, C. Téllez, J. Coronas and C. Janiak, *Eur. J. Inorg. Chem.*, 2016, 4363–4367; (*c*) H. B. Tanh Jeazet, C. Staudt and C. Janiak, *Dalton Trans.*, 2012, **41**, 14003–14027.

8 B. Chen, Z. Yang, Y. Zhu and Y. Xia, *J. Mater. Chem. A*, 2014, **2**, 16811–16831.

9 (*a*) J. Cravillon, C. A. Schröder, R. Nayuk, J. Gummel, K. Huber and M. Wiebcke, *Angew. Chem., Int. Ed.*, 2011, **50**, 8067–8071; (*b*) Z. Su, Y.-R. Miao, S.-M. Mao, G.-H. Zhang, S. Dillon, J. T. Miller and K. S. Suslick, *J. Am. Chem. Soc.*, 2015, **137**, 1750–1753; (*c*) K. C. Jayachandrababu, R. J. Verploegh, J. Leisen, R. C. Nieuwendaal, D. S. Sholl and S. Nair, *J. Am. Chem. Soc.*, 2016, **138**, 7325–7336; (*d*) S. B. Novaković, G. A. Bogdanović, C. Heering, G. Makhloufi, D. Francuski and C. Janiak, *Inorg. Chem.*, 2015, **54**, 2660–2670.

10 (*a*) C. J. Stephenson, J. T. Hupp and O. K. Farha, *Inorg. Chem.*, 2016, **55**, 1361–1363; (*b*) M. B. Lalonde, J. E. Mondloch, P. Deria, A. A. Sarjeant, S. S. Al-Juaid, O. I. Osman, O. K. Farha and J. T. Hupp, *Inorg. Chem.*, 2015, **54**, 7142–7144.

11 (*a*) C. Gücüyener, J. van den Bergh, J. Gascon and F. Kapteijn, *J. Am. Chem. Soc.*, 2010, **132**, 17704–17706; (*b*) C. Zhang, R. P. Lively, K. Zhang, J. R. Johnson, O. Karvan and W. J. Koros, *J. Phys. Chem. Lett.*, 2012, **3**, 2130–2134; (*c*) H. Bux, C. Chmelik, R. Krishna and J. Caro, *J. Membr. Sci.*, 2011, **369**, 284–289; (*d*) H. T. Kwon and H.-K. Jeong, *Chem. Commun.*, 2013, **49**, 3854–3856; (*e*) M. Askari and T. S. Chung, *J. Membr. Sci.*, 2013, **444**, 173–183; (*f*) C. Chmelik, D. Freude, H. Bux and J. Haase, *Microporous Mesoporous Mater.*, 2012, **147**, 135–141; (*g*) K. Li, D. H. Olson, J. Seidel, T. J. Emge, H. Gong, H. Zeng and J. Li, *J. Am. Chem. Soc.*, 2009, **131**, 10368–10369; (*h*) U. Böhme, B. Barth, C. Paula, A. Kuhnt, W. Schwieger, A. Mundstock, J. Caro and M. Hartmann, *Langmuir*, 2013, **29**, 8592–8600; (*i*) M. Hartmann, U. Böhme, M. Hovestadt and C. Paula, *Langmuir*, 2015, **31**, 12382–12389; (*j*) D. Peralta, G. Chaplais, A. Simon-Masseron, K. Barthelet, C. Chizallet, A. A. Quoineaud and G. D. Pirngruber, *J. Am. Chem. Soc.*, 2012, **134**, 8115–8126.

12 E. Bloch, W. L. Queen, R. Krishna, J. M. Zadrozny, C. M. Brown and J. R. Long, *Science*, 2012, **335**, 1606–1610.

13 N. Rosenbach Jr., A. Ghoufi, I. Deroche, P. L. Llewellyn, T. Devic, S. Bourrelly, C. Serre, G. Ferey and G. Maurin, *Phys. Chem. Chem. Phys.*, 2010, **12**, 6428–6437.

14 (*a*) K. P. Rao, M. Higuchi, K. Sumida, S. Furukawa, J. Duan and S. Kitagawa, *Angew. Chem., Int. Ed.*, 2014, **53**, 8225–8230;

(*b*) C. Yang, X. Wang and M. A. Omary, *J. Am. Chem. Soc.*, 2007, **129**, 15454–15455; (*c*) C. Yang, X. Wang and M. A. Omary, *Angew. Chem., Int. Ed.*, 2009, **48**, 2500–2505; (*d*) C. Yang, U. Kaipa, Q. Z. Mather, X. Wang, V. Nesterov, A. F. Venero and M. A. Omary, *J. Am. Chem. Soc.*, 2011, **133**, 18094–18097; (*e*) T.-H. Chen, I. Popov, W. Kaveevivitchai, Y.-C. Chuang, Y.-S. Chen, A. J. Jacobson and O. Š. Miljanić, *Angew. Chem., Int. Ed.*, 2015, **54**, 13902–13906; (*f*) P. Pachfule, Y. Chen, J. Jiang and R. Banerjee, *Chem. – Eur. J.*, 2012, **18**, 688–694; (*g*) S. Biswas, S. Couck, D. Denysenko, A. Bhunia, M. Grzywa, J. F. M. Denayer, D. Volkmer, C. Janiak and P. Van Der Voort, *Microporous Mesoporous Mater.*, 2013, **181**, 175–181; (*h*) P. Pachfule, Y. Chen, S. C. Sahoo, J. Jiang and R. Banerjee, *Chem. Mater.*, 2011, **23**, 2908–2916; (*i*) P. Pachfule, B. Garai and R. Banerjee, *Inorg. Chem.*, 2016, **55**, 7200–7205; (*j*) P. Pachfule, C. Dey, T. Panda and R. Banerjee, *CrystEngComm*, 2010, **12**, 1600–1609; (*k*) T. H. Chen, I. Popov, O. Zenasni, O. Daugulis and O. S. Miljanic, *Chem. Commun.*, 2013, **49**, 6846–6848.

15 (*a*) W.-W. Zhan, Q. Kuang, J.-Z. Zhou, X.-J. Kong, Z.-X. Xie and L.-S. Zheng, *J. Am. Chem. Soc.*, 2013, **135**, 1926–1933; (*b*) S. M. Meckler, C. Li, W. L. Queen, T. E. Williams, J. R. Long, R. Buonsanti, D. J. Milliron and B. A. Helms, *Chem. Mater.*, 2015, **27**, 7673–7679; (*c*) P. L. Feng, J. J. Perry IV, S. Nikodemski, B. W. Jacobs, S. T. Meek and M. D. Allendorf, *J. Am. Chem. Soc.*, 2010, **132**, 15487–15489.

16 Crystal data for CP-1: $C_6H_{6.5}F_3N_{2.5}O_2Zn$, Mr = 268.01 g mol^{-1}, crystal dimensions 1.00 × 0.42 × 0.11 mm, orthorhombic, space group *Pnma* (No. 62), a = 14.2627(4), b = 13.4623(5), c = 9.8745(7) Å, V = 1895.99(16) Å^3, Z = 8, ρ_{calcd} = 1.878 g cm^{-1}; $\mu(Mo_{K\alpha})$ = 2.617 mm^{-1} (λ = 0.71073 Å), T = 210 K; $2\Theta_{max}$ = 25.00°, 13168 reflections measured, 1740 unique (R_{int} = 0.0465), R_1 = 0.0240, wR = 0.0650 ($I > 2\sigma(I)$).

17 Crystal data for ZIF-318: $C_{18}H_{24.5}F_{4.5}N_8O_2Zn_{1.5}$, Mr = 568.51 g mol^{-1}, crystal dimensions 0.17 × 0.16 × 0.09 mm, cubic group $I\bar{4}3m$ (No 230), a = 40.0786(6) Å, V = 4981.5(5) Å^3, Z = 8, ρ_{calcd} = 1.516 g cm^{-1}; $\mu(Mo_{K\alpha})$ = 1.52 mm^{-1} (λ = 0.71073 Å), T = 180 K; $2\Theta_{max}$ = 24.92°, 16222 reflections measured, 848 unique (R_{int} = 0.0637), R_1 = 0.0383, wR = 0.0976 ($I > 2\sigma(I)$).

18 (*a*) K. S. W. Sing, D. H. Everett, R. A. Haul, L. Moscou, R. A. Pierotti, J. Rouquerol and T. Siemieniewska, *Pure Appl. Chem.*, 1985, **57**, 603–619; (*b*) M. Thommes, K. Kaneko, A. V. Neimark, J. P. Olivier, F. Rodriguez-Reinoso, J. Rouquerol and K. S. W. Sing, *Pure Appl. Chem.*, 2015, **87**, 1051–1069.

19 (*a*) F. Jeremias, A. Khutia, S. K. Henninger and C. Janiak, *J. Mater. Chem.*, 2012, **22**, 10148–10151; (*b*) F. Jeremias, D. Fröhlich, C. Janiak and S. K. Henninger, *New J. Chem.*, 2014, **38**, 1846–1852.

20 F. Jeremias, D. Fröhlich, C. Janiak and S. K. Henninger, *RSC Adv.*, 2014, **4**, 24073–24082.

21 (*a*) D. Fröhlich, S. K. Henninger and C. Janiak, *Dalton Trans.*, 2014, **43**, 15300–15304; (*b*) D. Fröhlich, E. Pantatosaki, P. D. Kolokathis, K. Markey, H. Reinsch, M. Baumgartner, M. A. van der Veen, D. E. De Vos, N. Stock, G. K. Papadopoulos, S. K. Henninger and C. Janiak, *J. Mater. Chem. A*, 2016, **4**, 11859–11869.

22 (*a*) J. Ehrenmann, S. K. Henninger and C. Janiak, *Eur. J. Inorg. Chem.*, 2011, **4**, 471–474; (*b*) S. K. Henninger, F. Jeremias, H. Kummer and C. Janiak, *Eur. J. Inorg. Chem.*, 2012, 2625–2634.

23 N. Nijem, P. Canepa, U. Kaipa, K. Tan, K. Roodenko, S. Tekarli, J. Halbert, I. W. H. Oswald, R. K. Arvapally, C. Yang, T. Thonhauser, M. A. Omary and Y. J. Chabal, *J. Am. Chem. Soc.*, 2013, **135**, 12615–12626.

24 (*a*) J.-S. Qin, S. Yuan, Q. Wang, A. Alsalme and H.-C. Zhou, *J. Mater. Chem. A*, 2017, **5**, 4280–4291; (*b*) Z. Yin, Y.-L. Zhou, M.-H. Zeng and M. Kurmoo, *Dalton Trans.*, 2015, **44**, 5258–5275.

25 (*a*) A. D. Burrows, C. G. Frost, M. F. Mahon and C. Richardson, *Angew. Chem., Int. Ed.*, 2008, **47**, 8482–8486; (*b*) K. Koh, A. G. Wong-Foy and A. J. Matzger, *Chem. Commun.*, 2009, 6162–6164; (*c*) W. Kleist, F. Jutz, M. Maciejewski and A. Baiker, *Eur. J. Inorg. Chem.*, 2009, 3552–3561; (*d*) W. Kleist, M. Maciejewski and A. Baiker, *Thermochim. Acta*, 2010, **499**, 71–78.

26 K. M. L. Taylor-Pashow, J. Della Rocca, Z. Xie, S. Tran and W. Lin, *J. Am. Chem. Soc.*, 2009, **131**, 14261–14263.

27 S. Nießing, C. Czekelius and C. Janiak, *Catal. Commun.*, 2017, **95**, 12–15.

28 S. Marx, W. Kleist, J. Huang, M. Maciejewski and A. Baiker, *Dalton Trans.*, 2010, **39**, 3795–3798.

29 J. Yang, Y. Zhang, Q. Liu, C. A. Trickett, E. Gutierrez-Puebla, M. Á. Monge, H. Cong, A. Aldossary, H. Deng and O. M. Yaghi, *J. Am. Chem. Soc.*, 2017, **139**, 6448–6455.